^{51}V Chemical Shielding and Quadrupole Coupling in Ortho- and Metavanadates from ^{51}V MAS NMR Spectroscopy

Jørgen Skibsted,[†] Claus J. H. Jacobsen,[‡] and Hans J. Jakobsen*,[†]

Instrument Centre for Solid-State NMR Spectroscopy, Department of Chemistry, University of Aarhus, DK-8000 Aarhus C, Denmark, and Haldor Topsøe Research Laboratories, DK-2800 Lyngby, Denmark

Received December 2, 1997

The combined effect from the ^{51}V quadrupole coupling and chemical shielding anisotropy (CSA) has been characterized for five orthovanadates ($Mg_3(VO_4)_2$, $Zn_3(VO_4)_2$, $BiVO_4$, $TaVO_5$, $NbVO_5$) and two metavanadates ($RbVO_3$ and $CsVO_3$) employing ^{51}V magic-angle spinning (MAS) NMR of the central and satellite transitions. Furthermore, five metavanadates studied earlier (MVO_3 where M = Li, Na, NH_4, Tl, K) have been reinvestigated using rotor-stabilized MAS NMR, which improves the reliability of the spinning sideband (ssb) intensities. The complete manifolds of ssbs from all seven single-quantum transitions, observed in the MAS NMR spectra, have been analyzed using least-squares fitting and numerical error analysis. The optimized data demonstrate that for the metavanadates the magnitudes of the quadrupole and shielding anisotropy tensors (i.e., C_Q, η_Q, δ_σ, η_σ) and of the Euler angle, which relates the principal element of the two tensors, can be determined with high precision. Somewhat larger error limits are observed for the two other Euler angles. The orthovanadates generally possess small shielding anisotropies which lead to a reduced precision of the CSA asymmetry parameter (η_σ). Relationships between the ^{51}V NMR data and structural parameters, crystal symmetries, and earlier reported correlations are discussed. Furthermore, linear correlations between the experimental principal elements of the ^{51}V quadrupole coupling tensors and estimated electric-field gradient tensor elements from point-monopole calculations are reported for both the ortho- and metavanadates.

Introduction

Solid-state NMR spectroscopy represents a valuable, often unique, technique in studies of catalytic support materials, surfaces, impregnated ions on these materials, and absorbed species on heterogeneous systems employing a range of different NMR nuclei (e.g. ^{1}H, ^{13}C, ^{27}Al, ^{29}Si, ^{31}P, ^{51}V, and ^{95}Mo) as structural probes.[1,2] As opposed to standard X-ray diffraction methods, solid-state NMR experiments provide structural information on the local environments of the NMR nuclei, which make the techniques extremely useful in characterizing complex catalytic systems where long-range order is absent. Recent years have witnessed an increasing interest in the use of ^{51}V NMR methods for studies of vanadates exhibiting catalytical properties[3−8] and of supported vanadium oxide catalysts.[7−14] Generally, these investigations aim at retrieving information on the vanadium environments from the isotropic ^{51}V chemical shifts (δ_{iso}) and/or the principal elements of the CSA tensors (δ_{xx}, δ_{yy}, and δ_{zz}). These parameters have been determined from either static-powder or magic-angle spinning (MAS) ^{51}V ($I = {}^7/_2$) NMR spectra of the central ($m = {}^1/_2 \leftrightarrow m = -{}^1/_2$) transition, utilizing the experimental fact that this transition is usually dominated by the CSA interaction at high magnetic fields.

Earlier we have shown that enhanced information on the local environments of the ^{51}V nuclei can be obtained from ^{51}V MAS NMR spectra by determination of the combined effect of the ^{51}V quadrupole coupling and CSA interactions from the complete manifold of spinning sidebands (ssbs) observed for the central and satellite transitions.[15,16] In addition to the magnitudes for the two interactions, i.e. the quadrupole coupling (C_Q and η_Q) and CSA (δ_σ and η_σ) parameters, the ssb intensities of the MAS NMR spectra also reflect the relative orientation of the quadrupole coupling and CSA tensors (i.e. the Euler angles ψ, χ, ξ). In certain cases these Euler angles may provide information about the orientation for some of the tensor components within the crystal structure. The first observation of noncoincident quadrupole coupling and CSA tensors was

* To whom correspondence should be addressed. Phone: +45 8942 3842. Fax: +45 8616 6199. E-mail: hja@kemi.aau.dk.
[†] University of Aarhus.
[‡] Haldor Topsøe Research Laboratories.

(1) Duncan, T. M.; Dybowski, C. R. *Surf. Sci. Rep.* **1981**, *1*, 157.
(2) *NMR Techniques in Catalysis*; Bell, A. T., Pines, A., Eds.; Marcel Dekker: New York, 1994.
(3) Hardcastle, F. D.; Wachs I. E.; Eckert, H.; Jefferson, D. A. *J. Solid State Chem.* **1991**, *90*, 194.
(4) Davis, J.; Tinet, D.; Fripiat, J. J.; Amarilla, J. M.; Casal, B.; Ruiz-Hitzky, E. *J. Mater. Res.* **1991**, *6*, 393.
(5) Crans, D. C.; Felty, R. A.; Chen, H.; Eckert, H.; Das, N. *Inorg. Chem.* **1994**, *33*, 2427.
(6) Luan, Z.; Xu, J.; Klinowski, J.; Kevan, L. *J. Phys. Chem.* **1996**, *100*, 19595.
(7) Eckert, H.; Wachs I. E. *J. Phys. Chem.* **1989**, *93*, 6796.
(8) Lapina, O. B.; Mastikhin, V. M.; Shubin, A. A.; Krasilnikov, V. N.; Zamaraev, K. I. *Prog. Nucl. Magn. Reson. Spectrosc.* **1992**, *24*, 457.
(9) Taouk, B.; Guelton, M.; Grimblot, J.; Bonnelle, J. P. *J. Phys. Chem.* **1988**, *92*, 6700.
(10) Le Coustumer, L. R.; Taouk, B.; Le Meur, M.; Payen, E.; Guelton, M.; Grimblot, J. *J. Phys. Chem.* **1988**, *92*, 1230.
(11) Chary, K. V. R.; Rao, V. V.; Mastikhin, V. M. *J. Chem. Soc., Chem. Commun.* **1989**, 202.
(12) Das, N.; Eckert, H.; Hu, H.; Wachs, I. E.; Walzer, J. F.; Feher, F. J. *J. Phys. Chem.* **1993**, *97*, 8240.
(13) Chary, K. V. R.; Kishan, G. *J. Phys. Chem.* **1995**, *99*, 14424.
(14) Mastikhin, V. M.; Terskikh, V. V.; Lapina, O. B.; Filimonova, S. V.; Seidl, M.; Knözinger, H. *Solid State Nucl. Magn. Reson.* **1995**, *4*, 369.
(15) Skibsted, J.; Nielsen, N. C.; Bildsøe, H.; Jakobsen, H. J. *Chem. Phys. Lett.* **1992**, *188*, 405.
(16) Skibsted, J.; Nielsen, N. C.; Bildsøe, H.; Jakobsen, H. J. *J. Am. Chem. Soc.* **1993**, *115*, 5, 7351.

S0020-1669(97)01503-6 CCC: $15.00
Published on Web 05/21/1998

reported in a ^{51}V single-crystal NMR study of V_2O_5.[17] The combined effect of the two ^{51}V tensor interactions has also been investigated by ^{51}V static-powder NMR for V_2O_5[8,18] and some metavanadates.[19] In the latter study, however, coincidence of the principal axis systems for the two tensors was assumed.[19] Most recently, ^{51}V off-MAS NMR has been used to describe the two tensor interactions for NH_4VO_3 and a vanadium nitrilotriacetate complex.[20] We also note that accurate determination of the isotropic chemical shift requires a preknowledge of quadrupole coupling parameters (or at least the product $C_Q(1 + \eta_Q^2)^{1/2}$), since the second-order quadrupolar shift of the central transition may result in nonnegligible low-frequency shifts of the resonances (e.g. shifts up ca. 6 ppm for ^{51}V at 9.4 T have been observed[16]). Although this fact has been ignored in several ^{51}V NMR studies, the second-order quadrupolar-induced shift should be considered when the isotropic chemical shifts are used quantitatively in correlations with structural parameters.

This work reports the determination of the magnitudes and relative orientations of ^{51}V quadrupole coupling and CSA tensors by MAS NMR for a series of orthovanadates ($Mg_3(VO_4)_2$, $Zn_3(VO_4)_2$, $BiVO_4$, $NbVO_5$, $TaVO_5$) and for the metavanadates $RbVO_3$ and $CsVO_3$. The latter two vanadates belong to the isostructural series of metavanadates MVO_3, where M = K, NH_4, Tl, Rb, Cs, and refined ^{51}V NMR data for the other members of this series (MVO_3, M = K, NH_4, Tl) studied earlier[16] and for $LiVO_3$ and α-$NaVO_3$ are also reported.

A preknowledge of accurate parameters for the ^{51}V quadrupole and CSA tensors in different types of vanadium species is important for unambiguously characterizing specific vanadium environments in vanadates and in supported vanadium oxide catalysts using ^{51}V NMR methods. Furthermore, improved information about the local electronic ^{51}V environments in these materials may be obtained, when relationships between NMR data and structural parameters (e.g. coordination states, polymerization degrees, electronegativities, bond angles and lengths) are established. For vanadates with V^{5+} in tetrahedral coordination Eckert and Wachs[7] have shown that the ^{51}V CSA increases with increasing degree of polymerization for ortho-, pyro-, and metavanadates. Moreover, Hayakawa *et al.*[21,22] have suggested that the state of coordination and degree of polymerization for VO_n polyhedra can be predicted on basis of the CSA parameters (δ_σ and η_σ). Thus, these authors reported correlations between δ_{iso} and the average V−O bond length[21] and between δ_{iso} and the electronegativity of the metal ion adjacent to the VO_4 tetrahedron.[22] The present work also includes a reinvestigation of these and related correlations[8,21,22] using the ^{51}V data determined for the ortho- and metavanadates in this work. Furthermore, relationships between ^{51}V quadrupole coupling parameters and structural data, reported from X-ray diffraction analysis, are investigated using point-monopole calculations which model the electronic structure at the nuclear site.

Experimental Section

NMR Measurements. Solid-state ^{51}V MAS NMR experiments were performed at 105.2 MHz (9.4 T) and 131.5 MHz (11.7 T) on Varian UNITY-400 and UNITY-500 spectrometers using home-built MAS probes[23] for 7 mm o.d. ceramic rotors allowing spinning speeds in the range 0.5−10 kHz with a stability of ±5 Hz to be employed. Improved stability (±1 Hz) of the spinning speed was achieved using a modified Varian Assoc. rotor-speed controller as described elsewhere.[24] All experiments were performed using exact magic-angle setting, spectral widths of 0.5−2.0 MHz, single-pulse excitation with a pulse width of 0.5−1.0 μs (for $\gamma H_1/2\pi \approx 50$ kHz), and a relaxation delay of 1 s. Baseline distortions were suppressed by linear prediction of the first few (5 to 15) data points of the FID followed by baseline correction using the routine of the Varian VNMR software. Isotropic chemical shifts (ppm) are reported relative to neat $VOCl_3$ using an external aqueous solution of 0.16 M $NaVO_3$ ($\delta_{iso} = -574.38$ ppm)[16] as secondary reference. However, for the ^{51}V MAS NMR spectra shown in the figures, the kHz scale is given relative to the isotropic peak in order to appreciate the asymmetry of the ssb manifolds.

Simulation Software. Simulations, least-squares fittings, and error analyses of the experimental MAS NMR spectra were performed on the SUN Sparc 10/51 workstation of the UNITY-400 spectrometer using the solid-state NMR software package STARS (SpecTrum Analysis of Rotating Solids) developed in our laboratory[15,16,24−26] and incorporated into the Varian VNMR software. The parameters characterizing the anisotropic parts and the relative orientation of the quadrupole coupling and CSA tensors (i.e. C_Q, η_Q, δ_σ, η_σ, ψ, χ, ξ) are obtained from least-squares optimizations of simulated to integrated ssb intensities for all seven ^{51}V single-quantum transitions observed in the experimental MAS spectra. The simulation program calculates the contributions from the first- and second-order quadrupolar and first-order CSA interactions in the secular approximation. However, for the actual spin systems (*e.g.* ^{51}V at 9.4 T) we find that the contribution from the second-order quadrupolar interaction can be neglected in the calculations used for optimizations to integrated ssb intensities. The effect from nonuniform detection (i.e. the quality factor Q of the probe circuitry)[25] has been included in the simulations while the intensity distortions caused by nonideal excitation[25] are negligible for the spin systems considered here, when small radio frequency pulse widths and strong radio frequency field strengths are employed. The quadrupole coupling and CSA parameters are given by

$$C_Q = eQV_{zz}, \quad \eta_Q = (V_{yy} - V_{xx})/V_{zz}, \quad \delta_\sigma = \delta_{iso} - \delta_{zz}, \quad \eta_\sigma = (\delta_{xx} - \delta_{yy})/\delta_\sigma \quad (1)$$

where $\delta_{iso} = {}^1/_3(\delta_{xx} + \delta_{yy} + \delta_{zz})$ and the principal elements of the CSA (δ) and electric field-gradient (**V**) tensors are defined using the convention[27] $|\lambda_{zz} - {}^1/_3\mathrm{Tr}(\lambda)| \geq |\lambda_{xx} - {}^1/_3\mathrm{Tr}(\lambda)| \geq |\lambda_{yy} - {}^1/_3\mathrm{Tr}(\lambda)|$ for $\lambda = \delta, V$. The Euler angles (ψ, χ, ξ), relating the principal axis system of the quadrupole coupling and CSA tensors, correspond to positive rotations around the z axis (ψ), the new y axis (χ), and the final z axis (ξ). ψ, χ, and ξ are given in the reduced ranges $0 \leq \psi \leq \pi$ and $0 \leq \chi, \xi \leq \pi/2$, caused by the symmetry of the first-order Hamiltonians for the quadrupole and CSA interactions and by the powder averaging of these expressions over all crystallite orientations. Expressions for the orientations that cannot be distinguished are given elsewhere.[16] The error limits for the optimized NMR parameters have been obtained by the method for numerical error analysis described in ref (24), which calculates the 95% confidence interval for a parameter from the curvature of a one-dimensional projection of the χ^2 surface in the direction of the parameter.

Materials. In all syntheses of vanadates reagents of analytical purity grade were employed without further purification. The basic structure and purity of all samples were checked by powder X-ray diffraction using the JCPDS diffraction files as reference.

(17) Gornostansky, S. D.; Stager, C. V. *J. Chem. Phys.* **1967**, *46*, 4959.
(18) France, P. W. *J. Magn. Reson.* **1991**, *92*, 30.
(19) Baugher, J. F.; Taylor, P. C.; Oja, T.; Bray, J. P. *J. Chem. Phys.* **1969**, *50*, 4914.
(20) Hayashi, S. *Magn. Reson. Chem.* **1996**, *34*, 791.
(21) Hayakawa, S.; Yoko, T.; Sakka, S. *J. Solid State Chem.* **1994**, *112*, 329.
(22) Hayakawa, S.; Yoko, T.; Sakka, S. *Bull. Chem. Soc. Jpn.* **1993**, *66*, 3393.
(23) Jakobsen, H. J.; Daugaard, P.; Langer, V. *J. Magn. Reson.* **1988**, *76*, 162; U.S. Patent 4,739,270, April 19, 1988.
(24) Skibsted, J.; Vosegaard, T.; Bildsøe, H.; Jakobsen, H. J. *J. Phys. Chem.* **1996**, *100*, 14872.
(25) Skibsted, J.; Nielsen, N. C.; Bildsøe, H.; Jakobsen, H. J. *J. Magn. Reson.* **1991**, *95*, 88.
(26) Vosegaard, T.; Skibsted, J.; Bildsøe, H.; Jakobsen, H. J. *J. Phys. Chem.* **1995**, *99*, 10731.
(27) Spiess, H. W. In *NMR Basic Principles and Progress*; Diehl, P., Fluck, E., Kosfeld, E., Eds.; Springer: Berlin, 1978; Vol. 15.

$Mg_3(VO_4)_2$. A 5.385 g (21 mmol) amount of magnesium nitrate hexahydrate ($Mg(NO_3)_2 \cdot 6H_2O$) was mixed with 1.273 g (7 mmol) of V_2O_5 in a platinum crucible. A 5 mL amount of concentrated nitric acid was added, and the suspension was stirred for 1 h and subsequently dried at 110 °C for 24 h. The resulting powder was calcined at 800 °C for 3 days.

$Zn_3(VO_4)_2$. A 6.247 g (21 mmol) amount of zinc nitrate hexahydrate ($Zn(NO_3)_2 \cdot 6H_2O$) was mixed with 1.276 g (7 mmol) of V_2O_5 in a platinum crucible. A 5 mL aliquot of concentrated nitric acid was added, and the suspension was stirred for 1 h and dried at 110 °C for 24 h. The yellowish powder was calcined at 600 °C for 5 days. ^{51}V MAS NMR showed that the sample contained a mixture of $Zn_3(VO_4)_2$ and α-$Zn_2V_2O_7$ in a molar ratio of ca. 1.0:0.5 (vide infra).

$BiVO_4$. A 3.881 g (8.0 mmol) amount of bismuth nitrate pentahydrate ($Bi(NO_3)_3 \cdot 5H_2O$) was mixed with 0.728 g (4.0 mmol) of V_2O_5 in a platinum crucible. A 5 mL aliquot of concentrated nitric acid was added, and the suspension was stirred for 1 h and subsequently dried at 110 °C for 24 h. The orange powder was calcined at 800 °C for 3 days.

$NbVO_5$. The preparation of $NbVO_5$ was based on a modification of the sol−gel synthesis developed by Maurer and Ko[28] for the preparation of high-surface area niobium(V) oxide. Amounts of 1.70 g (7.02 mmol) of $VO(C_3H_7O)_3$ and 2.23 g (7.02 mmol) of $Nb(OCH_2CH_3)_5$ were mixed by stirring in a 25 mL beaker containing 12.5 mL of 2-butanol. This solution was added with thorough stirring to a 50 mL beaker containing 12.5 mL of 2-butanol, 2.24 g (0.124 mmol) of water, and 0.60 mL concentrated nitric acid. Within half a minute a yellow gel formed, which was allowed to age for half an hour before evaporation to dryness in a rotatory evaporator at ca. 16 mmHg and 50 °C. This gave an olive green powder, which was calcined in flowing air at 550 °C for 6 h leaving a yellow product Isolated yield of $NbVO_5$: 1.47 g (94%).

$TaVO_5$. $TaVO_5$ was prepared by a method analogous to the synthesis of $NbVO_5$ with the difference that 2.85 g (7.02 mmol) of tantalum(V) ethoxide was used instead of niobium(V) ethoxide. The dried gel was calcined at 600 °C in flowing air for 8 h leaving a bright-yellow product. Isolated yield of $TaVO_5$: 2.12 g (97%).

Metavanadates. The preparation of the samples $LiVO_3$, NH_4VO_3, α-$NaVO_3$, KVO_3, and $TlVO_3$ has been described elsewhere,[16] while samples of $CsVO_3$ and $RbVO_3$ were prepared by reaction of cesium and rubidium carbonate with V_2O_5 using an earlier reported procedure.[29]

Results and Discussion

Determination of parameters for the ^{51}V quadrupole coupling and CSA interactions from ^{51}V MAS NMR spectra of the series of ortho- and metavanadates is described below for the individual samples. Where possible, the optimized parameters are compared with earlier reported values and relations between the NMR data and the ^{51}V point symmetries of the crystal structures are discussed. Furthermore, correlations between the NMR data and structural parameters, derived from the crystal structures reported from X-ray diffraction, are investigated.

$Mg_3(VO_4)_2$. The ^{51}V MAS NMR spectrum ($\nu_r = 4.0$ kHz) showing the complete manifold of ssbs from the central and satellite transitions for $Mg_3(VO_4)_2$ is illustrated in Figure 1a. The slight asymmetric features of the ssb envelope reflect the combined effect from the quadrupole coupling and CSA interaction while the ca. 5-fold larger intensity of the centerband relative to the first-order ssbs (*cf.* inset of Figure 1a) indicates that the central transition is only influenced by a relatively small ^{51}V CSA. Seven-parameter fits and error analyses of simulated to experimental ssb intensities for the spectrum in Figure 1a and additional spectra recorded at spinning speeds of 3.0 and 5.5 kHz (not shown) reveal that reliable values for the three

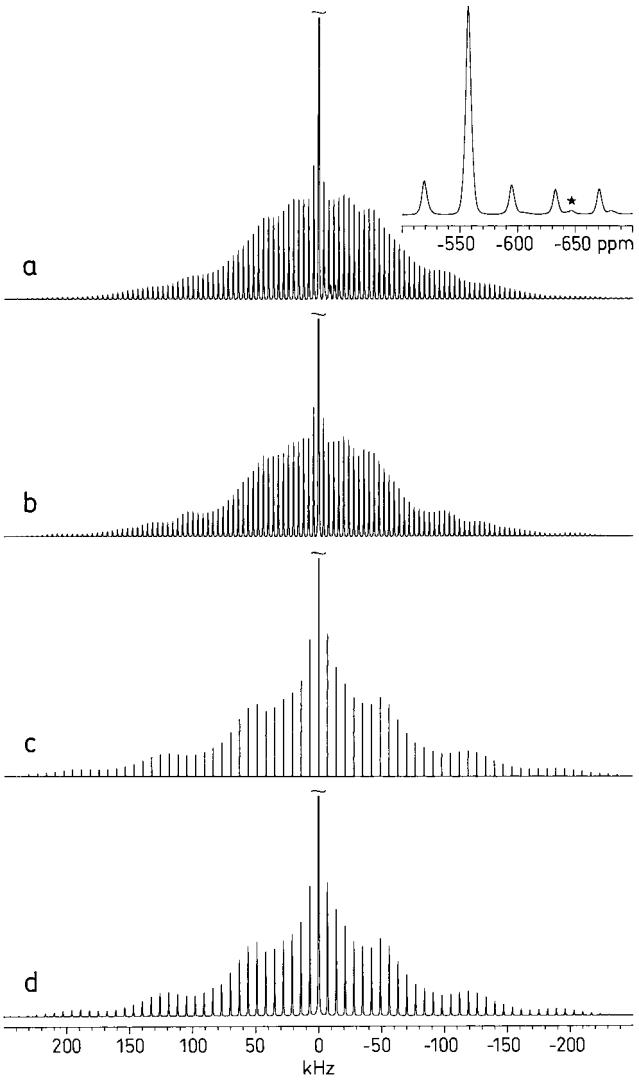

Figure 1. Experimental (a) and simulated (b) ^{51}V MAS NMR spectrum (9.4 T, $\nu_r = 4.0$ kHz) of the central and satellite transitions for $Mg_3(VO_4)_2$. The inset in (a) illustrates the ^{51}V central transition for $Mg_3(VO_4)_2$ on a full intensity scale and with a ppm scale given relative to neat $VOCl_3$, while the asterisk indicates the central transition from a minor impurity of β-$Mg_2V_2O_7$ in the sample. The simulation in (b) employs the optimized parameters for $Mg_3(VO_4)_2$ listed in Table 1 and a combination of Lorentzian and Gaussian line broadening, which results in ssb line widths of 520 Hz in agreement with those observed in the experimental spectrum. (c) Stick plot of experimental, integrated centerband, and ssb intensities for $Zn_3(VO_4)_2$ observed in the ^{51}V MAS NMR spectrum ($\nu_r = 7.0$ kHz) of the $Zn_3(VO_4)_2$ sample shown in Figure 2a. (d) Optimized simulation of the centerband and ssb intensities in (c) corresponding to the ^{51}V parameters for $Zn_3(VO_4)_2$ listed in Table 1. The central transition is cutoff at $^1/_4$ of its total height in (a and b) and at $^1/_3$ in (c and d).

Euler angles cannot be obtained from any of the spectra, an effect that may result from the small CSA. Thus, it is utilized in the optimizations that the unique VO_4 tetrahedron in the orthorhombic crystal structure of $Mg_3(VO_4)_2$ (space group *Cmca*)[30] exhibits a crystallographic mirror plane, which implies that one axis for each of the interaction tensors is perpendicular to this plane. This constraint is fulfilled when two of the Euler angles (ψ, χ, ξ) equal 0° modulo 90°. Using different combinations of the values for two of the Euler angles in least-squares optimizations give the lowest root mean square (rms) deviation between simulated and experimental ssb intensities

(28) Maurer, S. M.; Ko, E. *J. Catal.* **1992**, *135*, 125.
(29) Feigelson, R. S.; Martin, G. W.; Johnson, B. C. *J. Cryst. Growth* **1972**, *13/14*, 686.
(30) Krishnamachari, N.; Calvo, C. *Can. J. Chem.* **1971**, *49*, 1629.

Table 1. ^{51}V Quadrupole Couplings (C_Q, η_Q), Chemical Shielding Anisotropies (δ_σ, η_σ), Relative Orientations (ψ, χ, ξ) for the Two Tensorial Interactions, and Isotropic Chemical Shifts for a Series of Orthovanadates and for the Pyrovanadate α-$Zn_2V_2O_7$[a]

compound	C_Q (MHz)	η_Q	δ_σ (ppm)	η_σ	ψ (deg)	χ (deg)	ξ (deg)	δ_{iso}[b] (ppm)
$Mg_3(VO_4)_2$	1.05 ± 0.02	0.56 ± 0.02	31 ± 3	0.53 ± 0.23	0[c]	64 ± 10	85 ± 23	−557.3 ± 0.3
$Zn_3(VO_4)_2$	1.04 ± 0.02	0.99 ± 0.02	41 ± 4	0.68 ± 0.41	0[c]	61 ± 15	67 ± 25	−522.5 ± 0.5
$BiVO_4$	4.94 ± 0.02	0.36 ± 0.02	94 ± 3	0.32 ± 0.09	2 ± 41	90 ± 9	30 ± 7	−421.1 ± 0.5
$TaVO_5$	0.85 ± 0.02	0.28 ± 0.02	53 ± 4	0.24 ± 0.22	90[c]	37 ± 19	90[c]	−773.2 ± 0.3
$NbVO_5$	1.20 ± 0.05	0.39 ± 0.04	70 ± 4	0.17 ± 0.15	90[c]	25 ± 19	90[c]	−791.4 ± 0.5
α-$Zn_2V_2O_7$	3.97 ± 0.03	0.54 ± 0.02	−119 ± 3	0.69 ± 0.04	71 ± 60	10 ± 12	77 ± 24	−615.9 ± 0.5

[a] Optimized data from least-squares fits to the ssb intensities observed in ^{51}V MAS NMR spectra at 9.4 T. The error estimates are 95% confidence limits calculated for each parameter from the rms deviation between simulated and experimental ssb intensities using the procedure given in ref 24. [b] Isotropic chemical shift referenced to liquid $VOCl_3$. [c] Parameter fixed during optimization (see text).

for $\psi = 0°$. Thus, the parameters listed in Table 1 for $Mg_3(VO_4)_2$ result from six-parameter fits to the experimental ssb intensities using $\psi = 0°$ as a fixed value. The optimized data and error limits show that $\xi = 90°$ is within the experimental error and thereby the constraint indicated above for two of the Euler angles is fulfilled. The isotropic chemical shift determined for $Mg_3(VO_4)_2$ (Table 1) is in good agreement with earlier reported δ-values from ^{51}V MAS NMR of the central transition,[7,8,22] while some discrepancy is observed between the CSA parameters in Table 1 and those reported by Hayakawa et al. ($\delta_\sigma = 15$ ppm, $\eta_\sigma = 1.0$)[22] from static-powder ^{51}V NMR of the central transition at 9.4 T. We note that the inset of Figure 1a also illustrates the presence of a minor impurity with the isotropic peak at approximately −645 ppm, which is assigned to β-$Mg_2V_2O_7$ using the chemical shift reported earlier for this vanadate.[8]

$Zn_3(VO_4)_2$. The ^{51}V MAS NMR spectrum ($\nu_r = 7.0$ kHz) of the synthesized sample of $Zn_3(VO_4)_2$ is shown in Figure 2a and illustrates two overlapping manifolds of ssbs with centerbands at −526 and −623 ppm and approximate total intensities in a ratio of 1:0.5. Single-crystal XRD has shown that $Zn_3(VO_4)_2$ and $Mg_3(VO_4)_2$ are isostructural compounds.[31] Thus all VO_4 tetrahedra in $Zn_3(VO_4)_2$ are crystallographically equivalent, indicating that one of the two ssb patterns originates from an impurity phase. Stick plots of integrated ssb intensities for the high- and low-frequency sites in the ^{51}V MAS spectrum of our $Zn_3(VO_4)_2$ sample (Figure 2a) are shown in Figure 1c and Figure 2e, respectively. From the similarity in spectral width (and thereby quadrupole coupling) between the stick plot of ssb intensities in Figure 1c and the ssb manifold observed for $Mg_3(VO_4)_2$ (Figure 1a), the high-frequency site of Figure 2a is assigned to $Zn_3(VO_4)_2$, while the low-frequency, low-intensity site is ascribed to the impurity phase. Least-squares optimization and error analysis for the ssb intensities observed for $Zn_3(VO_4)_2$ (Figure 1c) gives the parameters in Table 1 and the optimum simulation shown in Figure 1d. In analogy to the optimization for $Mg_3(VO_4)_2$ a fixed value of $\psi = 0°$ was employed, because initial seven-parameter fits showed that reliable values for all three Euler angles cannot be obtained from the ssb manifold in Figure 1c. The isotropic chemical shift (Table 1) is in good agreement with the value $\delta_{iso} = -522$ ppm[7,22] reported earlier for $Zn_3(VO_4)_2$ from ^{51}V MAS NMR of the central transition, while improved data for the CSA parameters is obtained from the ssb intensities in Figure 1c compared to those estimated by Hayakawa et al. ($\delta_\sigma = 28$ ppm, $\eta_\sigma = 0.96$)[22] from ^{51}V static-powder NMR of the central transition.

A least-squares optimization and error analysis has also been performed for the ssb manifold (Figure 2e) observed for the impurity site in the $Zn_3(VO_4)_2$ sample and the final result is illustrated by the simulated manifold of ssbs for this site in Figure 2f. Furthermore, a total simulation including the ssbs from $Zn_3(VO_4)_2$ and from the impurity site is shown in Figure 2d. It is noted that the expansions of a set of ssbs shown in Figure 2b and 2d illustrate that the ssbs from the impurity phase partly split into two peaks as a result of the difference in second-order quadrupolar shift for the ($\pm^1/_2 \leftrightarrow \pm^3/_2$) and ($\pm^3/_2 \leftrightarrow \pm^5/_2$) transitions. A comparison of the optimized parameters for the impurity site with ^{51}V CSA parameters determined earlier clearly reveals that α-$Zn_2V_2O_7$ constitutes the additional phase in our sample. ^{51}V chemical shielding data for α-$Zn_2V_2O_7$ have been reported by Eckert and Wachs ($\delta_\sigma = -120$ ppm, $\eta_\sigma = 0.67$, $\delta_{iso} = -616$ ppm)[7] and Hayakawa et al. ($\delta_\sigma = -118$ ppm, $\eta_\sigma = 0.65$, $\delta_{iso} = -620$ ppm),[22] and these parameters are in good agreement with those obtained from optimization to the ssb intensities in Figure 2e (Table 1). The observation of Euler angles (describing the relative orientation of the two interaction tensors) that deviate from 0° modulo 90° is in accord with the monoclinic crystal structure of α-$Zn_2V_2O_7$ (space group *C*2/*c*) reported from X-ray diffraction,[32] since the ^{51}V site is not located on the 2-fold axis in this space group. The larger shielding anisotropy (δ_σ) and the larger quadrupole coupling, observed for α-$Zn_2V_2O_7$ as compared to the data for $Zn_3(VO_4)_2$, may reflect the more distorted electronic environments of the ^{51}V site in the pyrovanadate unit compared to ^{51}V in the isolated VO_4 tetrahedron of the orthovanadate.

$BiVO_4$. Bismuth vanadate occurs in nature as the mineral pucherite (orthorhombic, space group *Pnca*),[33] while high-temperature synthesis gives a ferroelastic, tetragonal phase of $BiVO_4$,[34] which transforms into a monoclinic form (space group *I2/b*)[35] below the ferroelastic transition temperature (528 K). The ^{51}V MAS NMR spectrum ($\nu_r = 8.2$ kHz) of monoclinic $BiVO_4$ is shown in Figure 3a and reveals a ssb pattern dominated by the quadrupole coupling interaction, since only vague asymmetries in the ssb intensities of the manifold are observed at the quite high spinning frequency required to resolve all resonances. The expansions from two different regions (insets in Figure 3a) illustrate the observation of separate peaks from the individual transitions and that the ssbs from the outer transitions ($m = \pm^5/_2$, $m = \pm^7/_2$) exhibit second-order quadrupolar line shapes, indicating a quite large quadrupole coupling for the ^{51}V site in $BiVO_4$. Least-squares fitting of simultated to integrated ssb intensities for the spectrum in Figure 3a gives the parameters listed in Table 1 and the optimum simulation shown in Figure 3b. Although second-order effects were not considered in the simulations used for the optimization, the simulated spectrum in Figure 3b also includes the second-order

(31) Gopal, R.; Calvo, C. *Can. J. Chem.* **1971**, *49*, 3056.
(32) Gopal, R.; Calvo, C. *Can. J. Chem.* **1973**, *51*, 1004.
(33) Qurashi, M. M.; Barnes, W. H. *Am. Mineral.* **1953**, *38*, 489.
(34) Bierlein, J. D.; Sleight, A. W. *Solid State Commun.* **1975**, *16*, 69.
(35) Sleight, A. W.; Chen. H.-Y.; Ferretti, A.; Cox, D. E. *Mater. Res. Bull.* **1979**, *14*, 1571.

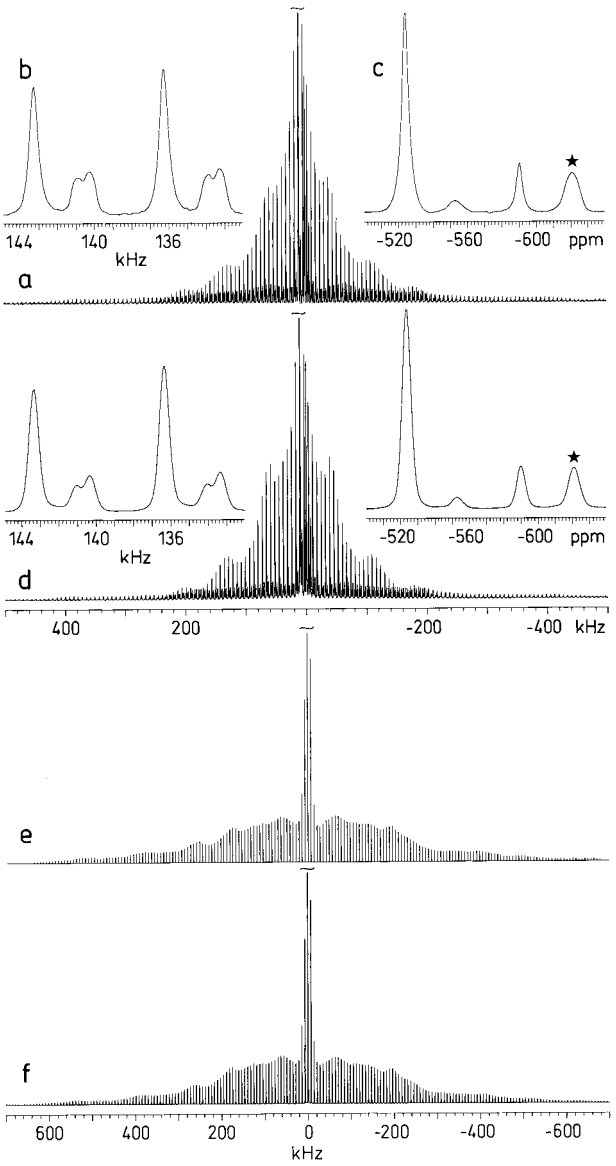

Figure 2. (a) ^{51}V MAS NMR spectrum (9.4 T, $\nu_r = 7.0$ kHz) of the central and satellite transitions observed for our $Zn_3(VO_4)_2$ sample, which consists of a mixture of $Zn_3(VO_4)_2$ and α-$Zn_2V_2O_7$. Expansion (b) illustrates that the low-intensity ssbs from α-$Zn_2V_2O_7$ partly split into separate peaks as a result of the difference in second-order quadrupolar shift of the individual transitions, while (c) shows the spectral region for the centerbands from $Zn_3(VO_4)_2$ and α-$Zn_2V_2O_7$ (asterisk) with a ppm scale relative to neat $VOCl_3$. Integrated centerband and ssb intensities for the two ^{51}V species are shown in Figure 1c for $Zn_3(VO_4)_2$ and in (e) for α-$Zn_2V_2O_7$. (d) Simulated spectrum including second-order quadrupolar effects of the ssb manifolds in (a) employing the ^{51}V parameters for $Zn_3(VO_4)_2$ and α-$Zn_2V_2O_7$ in Table 1 and an intensity ratio of $I(Zn_3(VO_4)_2)/I(\alpha\text{-}Zn_2V_2O_7) = 2.1$. The expansions in (d) correspond to those in (b) and (c) for the experimental spectrum. (f) Simulation of the centerband and ssb intensities in (e) for α-$Zn_2V_2O_7$ employing the optimized data in Table 1 for this phase.

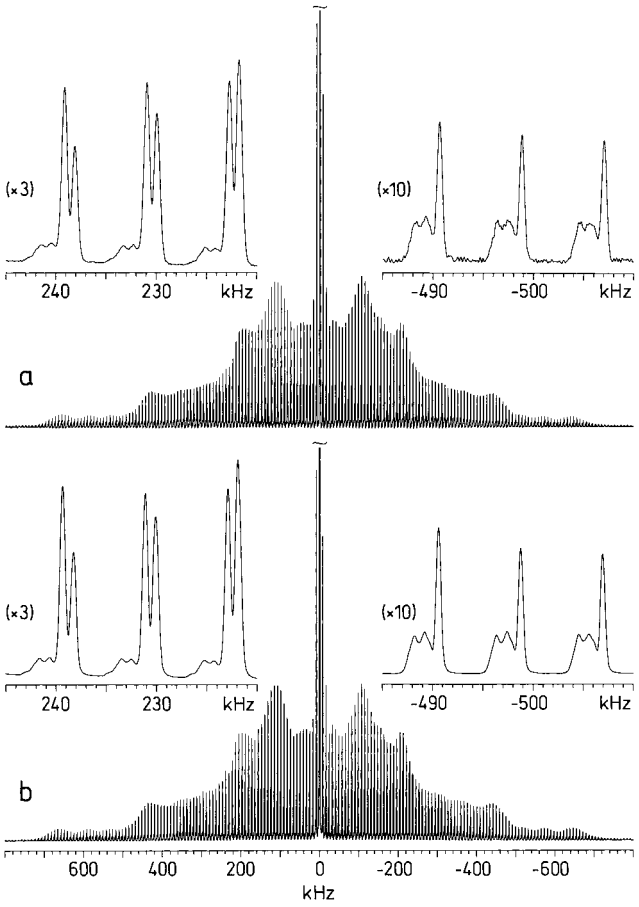

Figure 3. (a) Experimental ^{51}V MAS NMR spectrum of the central and satellite transitions for $BiVO_4$ recorded at 9.4 T using $\nu_r = 8.2$ kHz and 32.768 scans. (b) Simulated spectrum including the second-order quadrupolar broadening of the ssbs and employing the optimized parameters for $BiVO_4$ (Table 1) and a combination of 150 Hz Lorentzian and 200 Hz Gaussian line broadening for the ssbs. The insets for two regions in (a) and (b) illustrate the splitting of the ssbs caused by the difference in second-order quadrupolar shifts for the individual satellite transitions and the observation of resolved second-order quadrupolar line shapes for the outer ($\pm^5/_2 \leftrightarrow \pm^7/_2$) transitions (high-frequency side of the ssbs). The central transition is cutoff at about 30% of its total height in (a) and (b).

quadrupolar interaction in order to account for the line shapes of the ssbs. The excellent agreement between simulated and experimental ssb line shapes and intensities in Figure 3 shows that the experimental spectrum in Figure 3a represents probably the highest quality ^{51}V MAS NMR spectrum we have recorded to illustrate the ssb method for quadrupolar nuclei. The ^{51}V chemical shielding data in Table 1 may be compared with those reported by Eckert and Wachs ($\delta_\sigma = 81$ ppm, $\eta_\sigma = 0.58$, $\delta_{iso} = -423$ ppm)[7] and by Lapina et al. ($\delta_\sigma = 80$ ppm, $\eta_\sigma = 0.63$, $\delta_{iso} = -420$ ppm)[8] from ^{51}V static-powder and MAS NMR of the central transition. Furthermore, Hardcastle *et al.*[3] have reported values for the centers of gravity for the central transition of -432.1 ± 0.5 and -425.6 ± 0.5 ppm at 7.1 and 11.7 T, respectively. These values correspond to SOQE $= 5.2 \pm 0.2$ MHz and $\delta_{iso} = -421.5 \pm 0.7$ ppm, which are in good agreement with SOQE $= 5.05 \pm 0.05$ MHz and $\delta_{iso} = -421.1 \pm 0.5$ ppm determined from the ^{51}V MAS spectrum in Figure 3. The Euler angles relating the two interaction tensors (Table 1) are in accord with the location of the ^{51}V site on a 2-fold axis in the monoclinic structure for $BiVO_4$,[35] since $\psi = 0°$ and $\chi = 90°$ within experimental error. This corresponds to the principal elements of the CSA and quadrupole coupling tensors (σ_{zz} and V_{zz}) being mutually perpendicular and that one of them is parallel to the C_2 axis.

$TaVO_5$. The ^{51}V MAS NMR spectrum ($\nu_r = 4.4$ kHz) of the pentavalent metal orthovanadate $TaVO_5$ is shown in Figure 4a and illustrates an ssb manifold from a ^{51}V site possessing a small quadrupole coupling and small ^{51}V CSA. Initial seven-parameter fits to integrated intensities of the spectrum in Figure 4a show that the angles ψ and ξ are poorly defined from the experimental manifold of ssbs. The crystal structure for $TaVO_5$ (orthorhombic, space group *Pnma*), reported from powder XRD

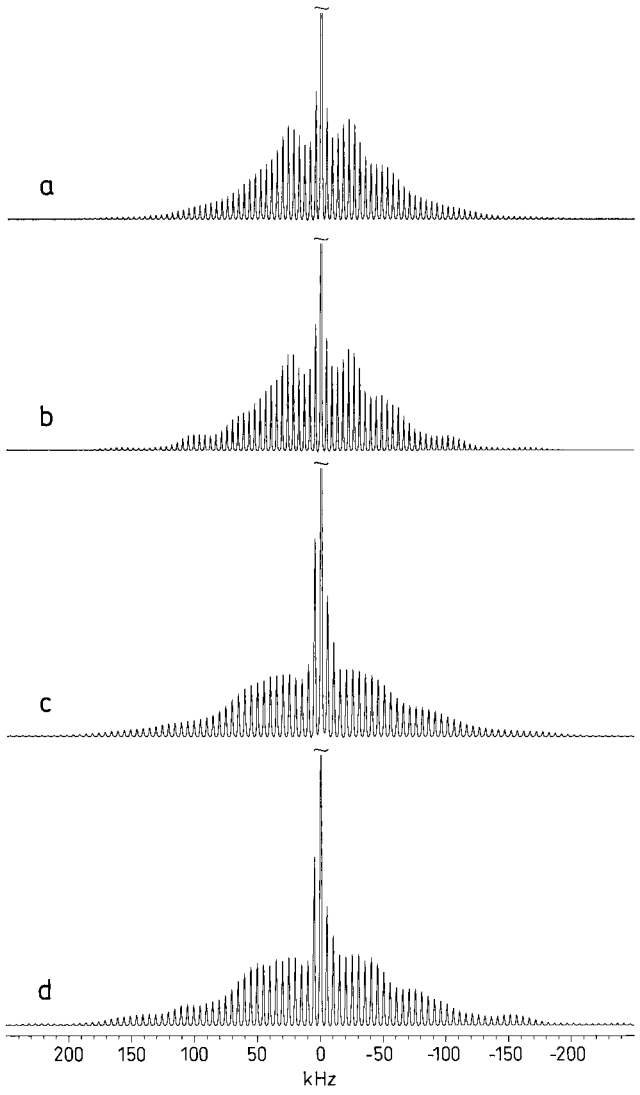

Figure 4. ^{51}V MAS NMR spectra of the central and satellite transitions for (a) $TaVO_5$ ($\nu_r = 4400$ Hz) and (c) $NbVO_5$ ($\nu_r = 5040$ Hz) obtained at 9.4 and 11.7 T, respectively. The corresponding simulated spectra are shown in (b) and (d) and employ the optimized parameters for $TaVO_5$ and $NbVO_5$ in Table 1 and a combination of Lorentzian and Gaussian line broadening, which results in ssb line widths of 800 Hz ($TaVO_5$) and 1200 Hz ($NbVO_5$), in agreement with those observed in the experimental spectra. The isotropic peak is cutoff at 33% of its total height in (a) and (b) and at half-height in (c) and (d).

data,[36] indicate that the ^{51}V site is located on a mirror plane, implying that two of the Euler angles should have a value of 0° or 90°. Consideration of this constraint using fixed ψ and ξ values of either 0° or 90° in five-parameter fits to the experimental data gives the lowest rms value for $\psi = \xi = 90°$. Employing these values gives the optimized values for the χ angle and the magnitudes of the two tensors listed in Table 1. The small values of η_σ and η_Q are a factor reducing the sensitivity of the ssb manifolds to changes in ψ and ξ. This fact comes from our observation that the magnitudes of η_σ and η_Q enter the specific terms in the expressions for first-order average Hamiltonians for the CSA and quadrupole interactions which describe the dependencies on ψ and ξ.[15] The manifold of experimental ssbs (Figure 4a) appears slightly smeared out when compared to the optimized simulation in Figure 4b. This most likely reflects that the sample is not highly crystalline in accordance with the method used for the synthesis, which is generally employed for the preparation of high surface area mixed metal oxides. Obviously, the observation may also be related to the low precision observed for the ψ and ξ angles.

$NbVO_5$. The mixed oxide $NbVO_5$ was synthesized for the first time in 1989 by Amarilla *et al.*[37] using sol−gel methods. From powder XRD analysis they observed that $NbVO_5$ is isostructural with $TaVO_5$, both having structures where the VO_4 tetrahedra share corners with $(Nb,Ta)O_6$ octahedra in an arrangement which give pentagonal channels along the *b* axis. The channels allow intercalation of alkali metals and with the aim of studying these intercalation processes by solid-state NMR, Davis *et al.*[4] have initially characterized $NbVO_5$ by ^{51}V and ^{93}Nb NMR. In that study they reported parameters for the magnitudes of the ^{51}V CSA and quadrupole coupling interactions ($C_Q = 1.0$ MHz, $\eta_Q = 0.2$, $\delta_\sigma = 73$ ppm, $\delta_\sigma = 0.27$, $\delta_{iso} = -789$ ppm) from static-powder and MAS NMR spectra of the central transition.[4] Improved ^{51}V interaction parameters are obtained from optimizations to the ssb manifolds observed in the ^{51}V MAS NMR spectrum ($\nu_r = 5.0$ kHz) of $NbVO_5$ shown in Figure 4c and in a spectrum recorded at lower spinning speed ($\nu_r = 3.3$ kHz, not shown). The optimized data (Table 1), illustrated by the simulated spectrum in Figure 4d, are achieved from five-parameter fits using the constraint $\psi = \xi = 90°$ in analogy to the optimization of the ^{51}V parameters for $TaVO_5$. The fact that $TaVO_5$ and $NbVO_5$ are isostructural compounds is clearly reflected by the optimized ^{51}V data (Table 1), which exhibit similarities for both the quadrupole coupling and CSA parameters.

Metavanadates. Recently, we reported magnitudes and relative orientations for the ^{51}V quadrupole coupling and chemical shielding tensors for five metavanadates (MVO_3, M = Li, Na, K, NH_4, Tl) from optimizations to ^{51}V MAS NMR spectra of the central and satellite transitions.[16] These metavanadates belong to two different isomorphous groups. $LiVO_3$ and α-$NaVO_3$ exhibit monoclinic lattices (space group $C2/c$)[38,39] while KVO_3, NH_4VO_3, and $TlVO_3$ have an orthorhombic structure (space group *Pbcm*).[40,41] The latter group of isomorphous metavanadates also includes $RbVO_3$ and $CsVO_3$ and to complete this group, ^{51}V NMR parameters for these two compounds have been determined in this work from analysis of the ^{51}V MAS NMR spectra shown in Figures 5 and 6.

The ^{51}V MAS spectrum of $RbVO_3$ (Figure 5a) illustrates the observation of the complete manifold of ssbs from the central and satellite transitions covering a spectral width of about 1.8 MHz. The inset of Figure 5a shows that separate peaks from the individual satellite transitions are observed and that the high-frequency shifted ssbs from the outer ($\pm 5/2 \leftrightarrow \pm 7/2$) transitions exhibit partly resolved second-order quadrupolar line shapes. Seven-parameter fits and error analysis of the ssbs in Figure 5a give the optimized parameters listed in Table 2, while the corresponding simulated spectrum is shown in Figure 5b. The simulation includes effects from the second-order quadrupolar interaction which results in an excellent fit to the line shapes and intensities of the ssbs in the experimental spectrum. The optimized ^{51}V parameters (Table 2) show that $RbVO_3$ exhibits the largest quadrupole coupling of the metavanadates and that the observed value agrees favorably with previously reported data ($C_Q = 4.33$ MHz and $\eta_Q = 0.72$).[8] However, the CSA

(36) Chahboun, H.; Groult, D.; Raveau, B. *Mater. Res. Bull.* **1988**, *23*, 805.
(37) Amarilla, J. M.; Casal, B.; Ruiz-Hitzky, *Mater. Lett.* **1989**, *8*, 132.
(38) Shannon, R. D.; Calvo, C. *Can. J. Chem.* **1973**, *51*, 265.
(39) Marumo, F.; Isobe, M.; Iwai, S.; Kondo, Y. *Acta Crystallogr.* **1974**, *B30*, 1628.
(40) Hawthorne, F. C.; Calvo, C. *J. Solid State Chem.* **1977**, *22*, 157.
(41) Ganne, M.; Piffard, Y.; Tournoux, M. *Can. J. Chem.* **1974**, *52*, 3539.

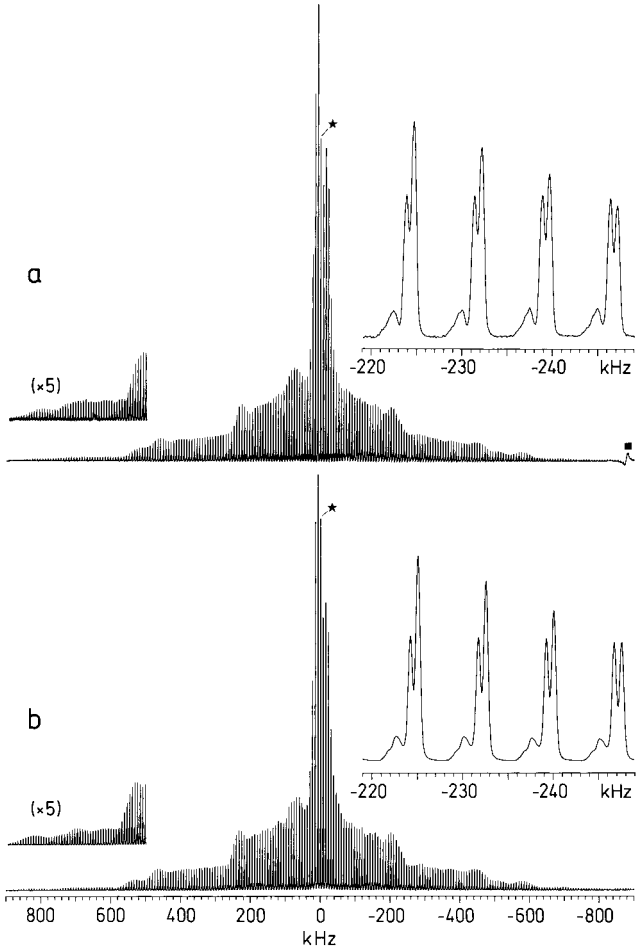

Figure 5. Experimental (a) and simulated (b) ^{51}V MAS NMR spectra (9.4 T, $\nu_r = 7.5$ kHz) of the central and satellite transitions for $RbVO_3$. The insets show the splitting of ssbs as a result of differences in second-order quadrupolar shift for the individual satellite transitions and the partly resolved second-order quadrupolar line shapes of the ssbs from the outer satellite transitions ($\pm^5/_2 \leftrightarrow \pm^7/_2$). The simulation includes the second-order quadrupolar interaction and employs the optimized parameters for $RbVO_3$ in Table 2 and a combination of 150 Hz Lorentzian and 200 Hz Gaussian line broadening for the ssbs. The centerband is marked by an asterisk while the square in (a) indicates the folded ^{63}Cu resonance from the radio frequency copper coil.

(δ_σ) in Table 2 is slightly larger than those reported by Lapina et al. ($\delta_\sigma = 293$ ppm, $\eta_\sigma = 0.67$, and $\delta_{iso} = -570$ ppm)[8] and by Hayashi and Hayamizu ($\delta_\sigma = 295$ ppm, $\eta_\sigma = 0.71$, and $\delta_{iso} = -569.1$ ppm)[42] from static-powder and MAS NMR spectra of the central transition. The high-frequency shift of approximately 4 ppm for δ_{iso} in Table 2, as compared to the values listed above, reflect that the earlier reported data have not been corrected for the second-order quadrupolar induced shift of the central transition.

The ^{51}V MAS spectrum of $CsVO_3$ in Figure 6a bears a close resemblance to the spectrum observed for $RbVO_3$ (Figure 5a), which indicates the presence of very similar ^{51}V environments in these two vanadates. A comparison of the optimized ^{51}V data for $CsVO_3$ (Table 2), resulting from least-squares optimization to the ssb intensities in Figure 6a, with those obtained for $RbVO_3$ supports this finding, since almost identical shielding anisotropies and only small variations in quadrupole coupling parameters are observed for the two metavanadates. The quadrupole coupling in Table 2 for $CsVO_3$ is slightly larger than the values reported earlier by Segel and Creel ($C_Q = 3.92 \pm 0.14$ MHz, $\eta_Q = 0.62 \pm 0.11$)[43] and by Pletnev et al. ($C_Q = 3.84 \pm 0.14$ MHz, $\eta_Q = 0.63 \pm 0.11$)[44] from static powder NMR. Furthermore, a somewhat larger shielding anisotropy and a high-frequency shift of δ_{iso} are observed, when the values in Table 2 are compared with the earlier reported data by Lapina et al. ($\delta_\sigma = 291$ ppm, $\eta_\sigma = 0.66$, $\delta_{iso} = -583$ ppm),[8] Hayashi and Hayamizu ($\delta_\sigma = 293$ ppm, $\eta_\sigma = 0.61$, $\delta_{iso} = -582.6$ ppm),[42] and Hayakawa et al. ($\delta_\sigma = 285$ ppm, $\eta_\sigma = 0.62$, $\delta_{iso} = -579$ ppm)[21] from static-powder and MAS NMR of the central transition. Again, the high-frequency shift of δ_{iso} is ascribed to the consideration of the second-order quadrupolar induced shift in this work.

Since the earlier study of the metavanadates (MVO_3, M = Li, Na, K, NH_4, Tl),[16] our techniques for extracting quadrupole coupling and CSA parameters from MAS NMR spectra of all transitions has been slightly improved by using rotor-speed control, because even an instability of a few Hz during the experiment may smear out the ssbs in especially the outer regions of the spectrum. Therefore we have reexamined the five metavanadates (MVO_3, M = Li, Na, K, NH_4, Tl) using this additional instrumentation and optimized ^{51}V parameters from seven-parameter least-squares fits to the experimental ssb intensities in these spectra are listed in Table 2 along with calculated error limits. Within the error limits the data in Table 2 agree with those given in our original investigation.[16] However, the error limits for the Euler angles ψ and ξ in Table 2 are generally somewhat larger than those reported in the earlier study,[16] despite the fact that the present spectra are of higher quality. The reason is that in the earlier work the error limits were estimated by visual comparison of experimental and a series of simulated spectra for which only one parameter was varied at a time. The improved numerical error analysis, employed in this work and described in ref 24, accounts for the larger errors observed in this study (Table 2) for the ψ and ξ values. For the orthorhombic series of metavanadates it is observed that the Euler angles $\psi = 90°$ and $\xi = 0°$ are within the experimental error in accordance with the requirement imposed by the crystal structures,[40,41] which show that the ^{51}V sites are situated in mirror planes. For the monoclinic $LiVO_3$ and α-$NaVO_3$ metavanadates no restrictions on the orientation of the quadrupole and CSA tensors are imposed by the crystal symmetry.

Relationships between the ^{51}V NMR Parameters and Crystal Structure Data. Correlations between quadrupole coupling constants and estimated values for the principal elements of the electric-field gradient (EFG) tensors ($\mathbf{V}^{est}$) at the nuclear site have recently been reported for tetrahedrally coordinated ^{27}Al sites in calcium aluminates,[45] for ^{23}Na in a series of sodium compounds,[46] and for ^{133}Cs in various cesium salts.[24] In these investigations the EFG tensor elements were obtained by point-monopole calculations,[47] which only consider oxygen anions within the first coordination sphere of the NMR nucleus. The correlations for the sodium and cesium compounds[24,46] employed effective charges for the oxygen anions obtained as $q_i = (-2 + \Sigma f_{ij})e$, where f_{ij} is the covalence of the oxygen (i)−cation (j) bond calculated from the equations of

(42) Hayashi, S.; Hayamizu, *Bull. Chem. Soc. Jpn.* **1990**, *63*, 961.
(43) Segel, S. L.; Creel, R. B. *Can. J. Phys.* **1970**, *48*, 2673.
(44) Pletnev, R. N.; Gubanov, V. A.; Chirkov, A. K. *Zh. Struct. Khim.* **1976**, *17*, 938.
(45) Skibsted, J.; Henderson, E.; Jakobsen, H. J. *Inorg. Chem.* **1993**, *32*, 1013.
(46) Koller, H.; Engelhardt, G.; Kentgens, A. P. M.; Sauer, J. *J. Phys. Chem.* **1994**, *98*, 1544.
(47) Cohen, M. H.; Reif, F. *Solid State Phys.* **1957**, *5*, 321.

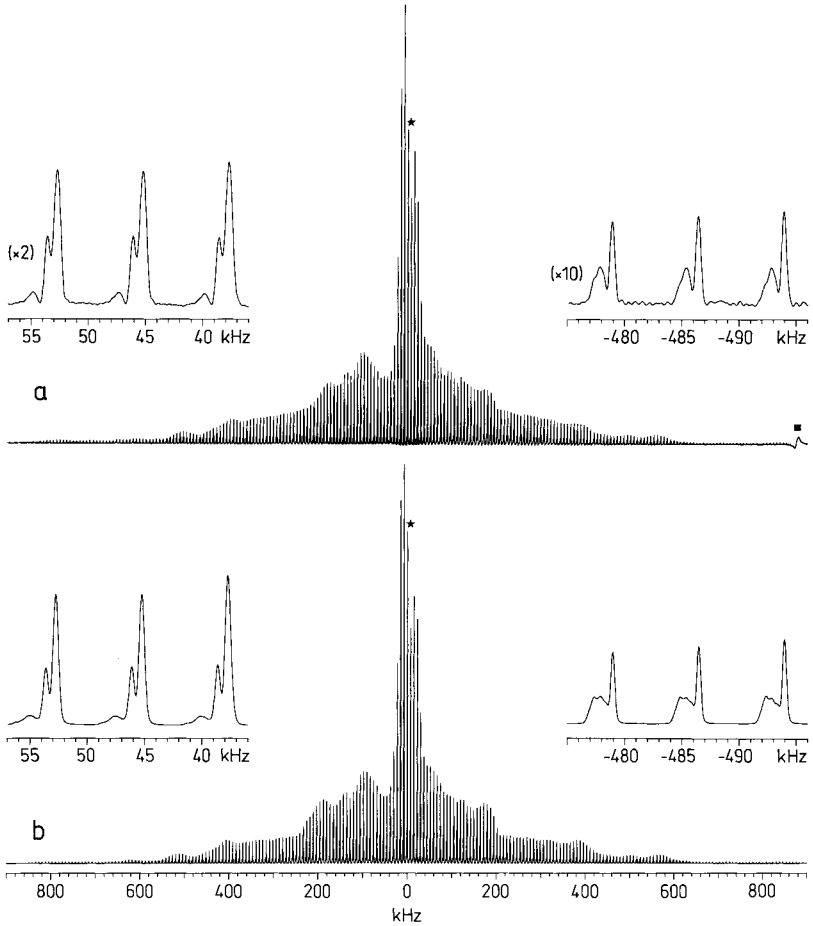

Figure 6. (a) Experimental ^{51}V MAS NMR spectrum (9.4 T, $\nu_r = 7.5$ Hz) of $CsVO_3$ illustrating the complete manifold of ssbs from the central and satellite transitions observed over a spectral width of 1.8 MHz. (b) Simulated spectrum of the ssbs in (a) including the contribution from the second-order quadrupolar interaction and using the optimized ^{51}V data in Table 2 for $CsVO_3$. A combination of 100 Hz Lorentzian and 150 Hz Gaussian line broadening was employed for the ssbs. The centerband is marked by an asterisk while the square in (a) indicates the folded ^{63}Cu resonance from the radio frequency copper coil. The small difference in second-order quadrupolar line shapes for the ssbs from the outer ($\pm^5/_2 \leftrightarrow \pm^7/_2$) satellite transitions, observed in the expansions of the simulated and experimental spectra, most likely reflects a small deviation from exact magic angle setting (less than ca. $\pm 0.02°$).

Table 2. ^{51}V Quadrupole Couplings (C_Q, η_Q), Chemical Shielding Anisotropies (δ_σ, η_σ), Relative Orientations (ψ, χ, ξ) for the Two Tensorial Interactions, and Isotropic Chemical Shifts for a Series of Metavanadates from ^{51}V MAS NMR[a]

compound	C_Q (MHz)	η_Q	δ_σ (ppm)	η_σ	ψ (deg)	χ (deg)	ξ (deg)	δ_{iso}[b] (ppm)
$LiVO_3$	3.25 ± 0.05	0.88 ± 0.02	228 ± 3	0.72 ± 0.02	105 ± 36	21 ± 10	72 ± 33	-573.2 ± 0.5
α-$NaVO_3$	3.77 ± 0.03	0.49 ± 0.02	249 ± 2	0.67 ± 0.02	156 ± 36	3 ± 11	75 ± 38	-572.8 ± 0.5
NH_4VO_3	2.98 ± 0.03	0.28 ± 0.02	245 ± 3	0.70 ± 0.02	76 ± 22	25 ± 6	13 ± 31	-569.5 ± 0.5
$TlVO_3$	3.76 ± 0.06	0.71 ± 0.03	267 ± 4	0.76 ± 0.03	106 ± 77	30 ± 7	9 ± 38	-529.1 ± 0.5
KVO_3	4.15 ± 0.04	0.85 ± 0.02	307 ± 3	0.66 ± 0.02	102 ± 35	8 ± 8	25 ± 28	-547.6 ± 0.5
$RbVO_3$	4.23 ± 0.03	0.64 ± 0.02	314 ± 2	0.69 ± 0.02	100 ± 35	28 ± 5	0 ± 26	-565.4 ± 0.2
$CsVO_3$	4.10 ± 0.03	0.48 ± 0.02	314 ± 2	0.67 ± 0.02	112 ± 60	21 ± 3	16 ± 26	-577.4 ± 0.2

[a] Optimized data from least-squares fits to the integrated ssb intensities in ^{51}V MAS NMR spectra. The error estimates are 95% confidence limits calculated for each parameter from the rms deviation between simulated and experimental ssb intensities using the procedure given in ref 24. [b] Isotropic chemical shift referenced to liquid $VOCl_3$.

Brown and Shannon[48] and from the chemical bond data of Brown and Altermatt.[49] The applicability of this approach for correlating ^{51}V quadrupole coupling parameters with estimated ^{51}V EFG tensor elements is investigated here for the studied ortho- and metavanadates. From the crystal structures for these vanadates, determined using single-crystal XRD,[30,31,35,38−41,50−54] estimated oxygen charges are calculated as described above and used in point-monopole calculations, which only consider the four oxygen anions in the first coordination sphere of the ^{51}V nuclear site. This gives the estimated values for the principal elements (V_{ii}^{est}) of the ^{51}V EFG tensors listed in Tables 3 and 4 for the ortho- and metavanadates, respectively. To expand the range of experimental values for the orthovanadates the analysis also includes data for $Sr_3(VO_4)_2$, $Ba_3(VO_4)_2$, Li_3VO_4, YVO_4, and $LaVO_4$ for which experimental quadrupole coupling parameters have been reported by Lapina et al.[8] However, $NbVO_5$

(48) Brown, I. D.; Shannon, R. D. *Acta Crystallogr. A* **1973**, *29*, 266.
(49) Brown, I. D.; Altermatt, D. *Acta Crystallogr. B* **1985**, *41*, 244.
(50) Süsse, P.; Buerger, M. J. *Z. Kristallogr.* **1970**, *131*, 161.
(51) Carrillo-Cabrera, W.; von Schnering, H. G. *Z. Kristallogr.* **1993**, *205*, 271.
(52) Shannon, R. D.; Calvo, C. *J. Solid State Chem.* **1973**, *6*, 538.
(53) Schmidt, G.; Deppisch, B.; Gramlich, V.; Scheringer, C. *Acta Crystallogr. B* **1973**, *29*, 141.
(54) Rice, C. E.; Robinson, W. R. *Acta Crystallogr. B* **1976**, *32*, 2232.

Table 3. ^{51}V Quadrupole Coupling Parameters (C_Q, η_Q) and estimated Principal Elements (V_{ii}^{est}) ($\times 10^{20}$ V m^{-2}) of the Electric Field Gradient Tensor for a Series of Orthovanadates[a]

compound	C_Q[b] (MHz)	η_Q[b]	V_{xx}^{est}	V_{yy}^{est}	V_{zz}^{est}	structure ref [d]
$Mg_3(VO_4)_2$			−0.249	−0.188	0.437	30
$Zn_3(VO_4)_2$			−0.197	−0.091	0.288	31
$BiVO_4$			−1.423	−0.345	1.768	35
$Ba_3(VO_4)_2$	0.75	*c*	−0.121	−0.121	0.242	50
$Sr_3(VO_4)_2$	0.53	*c*	−0.041	−0.035	0.077	51
Li_3VO_4	1.52	*c*	−0.341	−0.281	0.621	52
YVO_4	4.75	0.00	−1.360	−1.360	2.719	53
$LaVO_4$	5.21	0.69	−1.770	−0.499	2.269	54

[a] Estimated principal elements of the EFG tensor from a point-monopole calculation using effective charges for the oxygens surrounding the vanadium ion (see text). [b] Experimental quadrupole coupling parameters taken from ref 8. The C_Q and η_Q values for $Mg_3(VO_4)_2$, $Zn_3(VO_4)_2$, and $BiVO_4$ are given in Table 1. [c] Asymmetry parameter not reported. [d] References for the X-ray diffraction structure determinations, which provide the atomic coordinates for the point-monopole calculations.

Table 4. Estimated Principal Elements (V^{est}_{ii}) ($\times 10^{20}$ V m^{-2}) of the ^{51}V Electric Field Gradient Tensor for the Series of Metavanadates[a]

compound	V_{yy}^{est}	V_{yy}^{est}	V_{zz}^{est}	structure ref[b]
$LiVO_3$	−1.272	−0.349	1.621	38
α-$NaVO_3$	−1.586	−0.008	1.594	39
$TlVO_3$	−1.569	−0.136	1.705	41
KVO_3	−1.693	−0.579	2.272	40
$RbVO_3$	−1.446	−0.521	1.967	40
$CsVO_3$	−1.499	−0.340	1.839	40

[a] Estimated values from a point-monopole calculation using effective charges for the oxygens surrounding the vanadium ion (see text). [b] References for the X-ray diffraction structure determinations, which provide the atomic coordinates for the point-monopole calculations.

and $TaVO_5$ are not included in the analysis because the crystal structure for $NbVO_5$ has not been reported and because the fractional atomic coordinates for $TaVO_5$, obtained from refinements of powder XRD data,[36] have quite low precision. Furthermore, NH_4VO_3 is not included in the analysis since the bond valence parameter (r_0) has not been reported for NH_4^+. This prevents calculation of the effective oxygen charges for this compound. For the vanadates considered here, the effective oxygen charges range between $q = -0.84$e (O(2) for $TlVO_3$) and $q = -1.13$e (O(1) for Li_3VO_4). The calculated EFG tensor elements are correlated with the corresponding elements of the quadrupole coupling tensor (Q_{ii}^{exp}) in Figure 7a and b for the ortho- and metavanadates, respectively, where the experimental quadrupole coupling tensor elements are derived from C_Q and η_Q according to

$$Q_{zz}^{exp} = C_Q Q_{yy}^{exp} = -\,^1/_2(1-\eta_Q)/C_Q Q_{xx}^{exp} = -\,^1/_2(1+\eta_Q)/C_Q \quad (2)$$

assuming a positive value for C_Q. For the orthovanadates linear regression analysis of the experimental Q_{ii}^{exp} values and the calculated V_{ii}^{est} data gives the equation

$$Q_{ii}^{exp}(\text{MHz}) = 2.17 V_{ii}^{est}(\times 10^{20}\ \text{V m}^{-2}) + 0.04 \quad (3)$$

with a correlation coefficient $R = 0.97$. A similar relationship is observed between Q_{ii}^{exp} and V_{ii}^{est} for the metavanadates, *i.e.*

$$Q^{exp}{}_{ii}(\text{MHz}) = 2.09 V^{est}{}_{ii}(\times 10^{20}\ \text{V m}^{-2}) \quad (4)$$

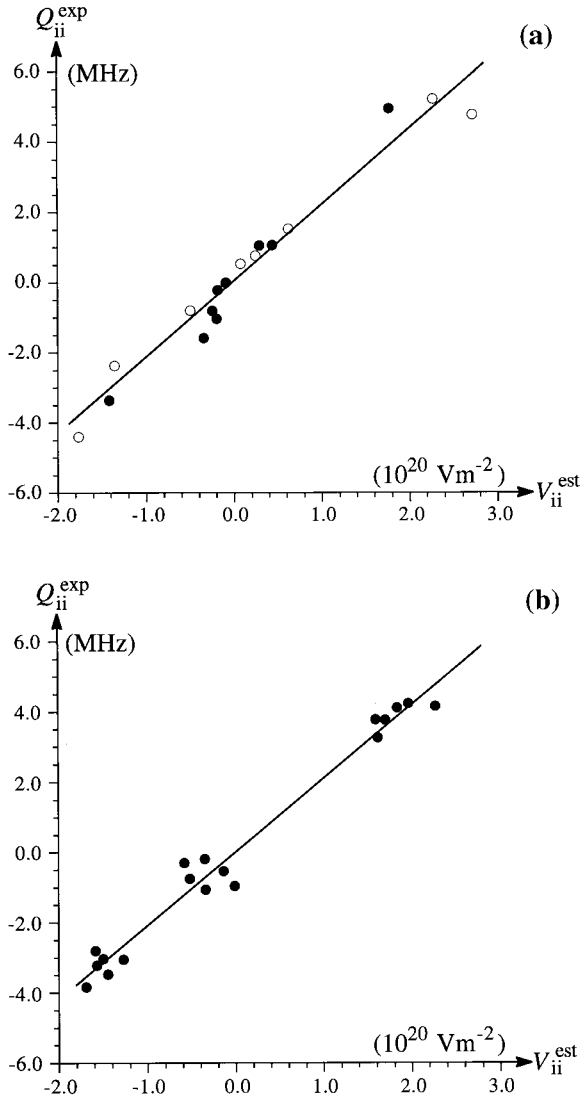

Figure 7. Linear correlations between ^{51}V quadrupole coupling tensor elements (Q_{ii}^{exp}) and estimated EFG tensors elements (V_{ii}^{est}) from a point-monopole calculation for (a) orthovanadates and (b) metavanadates. The calculated values for V_{ii}^{est} are summarized in Tables 3 and 4 while the results of linear regression analysis of the data are given in eqs 3 and 4 for the ortho- and metavanadates, respectively. The filled circles in (a) correspond to the orthovanadates studied in this work, while the open circles represent ^{51}V quadrupole coupling parameters reported in ref 8 for the orthovanadates $Ba_3(VO_4)_2$, $Sr_3(VO_4)_2$, Li_3VO_4, YVO_4, and $LaVO_4$ (*cf.* Table 3).

with a correlation coefficient $R = 0.98$. The almost identical slopes in eqs 3 and 4 suggest that the observed relationship between Q_{ii}^{exp} and V_{ii}^{est} may also be valid for other types of vanadates such as pyrovanadates. Calculation of the quadrupole coupling tensor elements (Q_{ii}^{exp}) from V_{ii}^{est} using eqs 3 and 4 results in average deviations between Q_{ii}^{est} and Q_{ii}^{exp} of 0.44 and 0.38 MHz for the ortho- and metavanadates, respectively. Thus, we expect that estimates of the quadrupole coupling tensor elements with a precision of approximately ±0.4 MHz may be achieved from point-monopole calculations of the EFG tensor elements using effective oxygen charges and eq 3 or 4.

Interpretation of the CSAs observed for the ortho- and metavanadates in terms of correlations with structural data appears less straightforward than for the quadrupole coupling parameters. However, the shielding anisotropy data in Tables 1 and 2 clearly reveal that the isolated VO_4^{3-} tetrahedra in the orthovanadates are associated with quite small CSAs ($31 \leq \delta_\sigma$

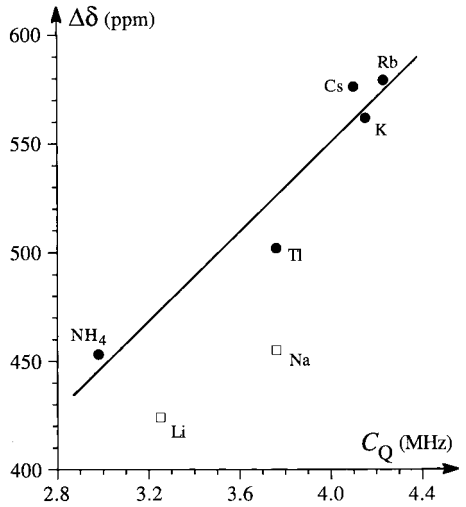

Figure 8. Correlation between ^{51}V quadrupole coupling constants and the magnitude of the chemical shielding anisotropies ($\Delta\delta = |\delta_{zz} - \delta_{xx}|$) for the studied metavanadates employing the experimental data in Table 2. The straight line illustrates the result of a linear regression analysis of the data for the isomorphous series of metavanadates (i.e. MVO_3 for M = NH_4, Tl, K, Rb, Cs). The open squares correspond to the parameters for $LiVO_3$ and α-$NaVO_3$ and have not been included in the regression analysis.

≤ 94 ppm), while significantly larger values are observed for the ^{51}V sites in the chains of VO_4^{3-} tetrahedra in the metavanadates (228 ≤ δ_σ ≤ 314 ppm). This finding is in agreement with earlier results by Eckert and Wachs,[7] who also found that dimeric $[O_3V-O-VO_3]^{4-}$ units in pyrovanadates exhibit δ_σ values between those observed for ortho- and metavanadates. From Table 2 it is also apparent that a CSA asymmetry parameter in the range 0.66 ≤ η_σ ≤ 0.76 is a characteristic feature for the metavanadates, which has been noted earlier by Hayakawa *et al.*[21] For the MVO_3 metavanadates where M = NH_4, Na, K, Rb, Cs, Lapina *et al.*[8] reported correlations between the magnitude of the CSA, defined by these authors as the parameter $\Delta\delta = |\delta_{zz} - \delta_{xx}|$, and the bridging O(3)−V−O(3)′ angle from X-ray diffraction and between $\Delta\delta$ and η_Q as well as $\Delta\delta$ and C_Q. However, the improved data for the CSA tensors and quadrupole coupling parameters reported here reveal that the correlations between $\Delta\delta$ and the bridging O(3)−V−O(3)′ angle as well as between $\Delta\delta$ and η_Q are less apparent. The depiction of $\Delta\delta$ versus C_Q in Figure 8 for the metavanadates studied shows the presence of an approximate linear correlation between these two parameters for the series of isostructural, orthorhombic metavanadates (i.e., MVO_3 for M = NH_4, Tl, K, Rb, Cs). Linear correlation of the data for this series of metavanadates gives the equation

$$\Delta\delta\ (\text{ppm}) = 103 C_Q\ (\text{MHz}) + 139 \qquad (5)$$

with a correlation coefficient $R = 0.96$. From Figure 8 it is also apparent that the $\Delta\delta$ and C_Q values for $LiVO_3$ and α-$NaVO_3$ do not fit the observed correlation for the orthorhombic metavanadates in contrast to the results reported by Lapina et al.[8] A linear relationship between the magnitudes of the CSA and quadrupole tensors has earlier been observed in ^{59}Co NMR for a series of Co(III) complexes,[55] while no simple relationship between δ_σ and C_Q was observed in a ^{133}Cs NMR study of some cesium salts.[56] These results and those obtained for the metavanadates indicate that correlations between δ_σ and C_Q may only be expected for quadrupoles in structurally related compounds.

Finally, it is noted that Hayakawa et al. have reported correlations between δ_{iso} and the average V−O bond length of the VO_4^{3-} tetrahedron for ortho-, pyro-, and monovalent metal metavanadates[21] and between δ_{iso} and the electronegativity of the metal cation adjacent to the VO_4 tetrahedron for divalent metal orthovanadates.[22] However, the δ_{iso} values for the studied ortho- and metavanadates in the present work show no correlation with the average V−O bond lengths, while δ_{iso} for $Mg_3(VO_4)_2$ and $Zn_3(VO_4)_2$ in Table 1 fit the reported correlation between δ_{iso} and the electronegativity of the metal cation for the $M_3(VO_4)_2$ (M = Pb, Mg, Zn, Sr, Ba) orthovanadates.[22] Since the chemical shielding tensor elements (or the parameters δ_σ and η_σ) reflect the local electronic environments of the ^{51}V nuclei much better than the isotropic chemical shift itself, we expect that the CSA parameters hold more promise in correlations with structural parameters such as V−O bond lengths, V−O−V bond angles, and effective cation charges.

Conclusions

The magnitudes and relative orientations of ^{51}V quadrupole coupling and chemical shielding tensors have been obtained for a series of ortho- and metavanadates employing rotor-stabilized MAS NMR of the central and satellite transitions. The magnitudes of the tensors (i.e. C_Q, η_Q, δ_σ, and η_σ) and the Euler angle χ between the principal element of the two tensors can be obtained with high precision for the metavanadates using this method, while the observed spinning sideband manifolds are rather insensitive to variations in the two other Euler angles (ψ and ξ). For the orthorhombic metavanadates, where the ^{51}V atom resides in a mirror plane, the values $\psi = 90°$ and $\xi = 0°$ are within the experimental error revealing that the principal elements of the CSA and EFG tensors are noncoincident and within the mirror plane. For the orthovanadates the small shielding anisotropies also prevent an accurate determination of the CSA asymmetry parameter (η_σ) at least from MAS NMR spectra obtained at a moderate magnetic field (9.4 T). Close similarities are observed for the magnitudes of the two tensors for the isostructural orthovanadates $Mg_3(VO_4)_2$ and $Zn_3(VO_4)_2$ as well as for $TaVO_5$ and $NbVO_5$. Linear correlations between the experimental principal elements of the ^{51}V quadrupole coupling tensor and a calculated estimate of the electric field gradient tensor, using the point-monopole approach, have been observed for the ortho- and metavanadates. These may be useful for the assignment of ^{51}V quadrupole couplings for samples with multiple vanadium sites and for estimation of quadrupole coupling parameters from crystal structure data. The correlation between C_Q and the magnitude of the CSA ($\Delta\delta = |\delta_{zz} - \delta_{xx}|$), observed for the isomorphous, orthorhombic series of metavanadates, serve to exemplify that simple relationships between the magnitudes of the quadrupole couplings and the chemical shielding anisotropies may be obtained only for structurally related compounds.

Acknowledgment. The use of the facilities at the Instrument Centre for Solid-State NMR Spectroscopy, University of Aarhus, sponsored by the Danish Research Councils (SNF and STVF), Teknologistyrelsen, Carlsbergfondet, and Direktør Ib Henriksens Fond, is acknowledged. We thank Aarhus University Research Foundation for equipment grants. Access to the use of the Varian UNITY-500 spectrometer at the University of Odense, Odense, Denmark, is greatly appreciated.

IC971503H

(55) Spiess, H. W.; Haas, H.; Hartmann, H., *J. Chem. Phys.* **1969**, *50*, 3057.
(56) Mooibroek, S.; Wasylishen, R. E.; Dickson, R.; Facey, G. *J. Magn. Reson.* **1986**, *66*, 542.